Modulated Standing Waves in a Short Reaction−Diffusion System

Milos Dolnik, Anatol M. Zhabotinsky,* and Irving R. Epstein

Department of Chemistry and Volen Center for Complex Systems, Brandeis University, Waltham, Massachusetts 02254-9110

Received: November 7, 1995; In Final Form: January 26, 1996[⊗]

We present a study of pattern formation beyond the onset of the wave instability in a short model reaction−diffusion system whose length is between 0.5 and 1.5 times the characteristic wavelength of the wave instability. As the system length is varied, modulated standing waves, characterized by short-lived alternating nodes, are found between the domains of the half-wavelength and the one-wavelength standing waves. The space−time two-dimensional Fourier spectra of these modulated standing waves show large side peaks. The position of these peaks differs from that of the fundamental peak by its wavenumber and by the frequency of appearance of the alternating nodes. Another region of modulated standing waves is found within the domain of standing−traveling waves.

Introduction

Pattern formation in reaction−diffusion systems has been a subject of intensive study for the past 40 years.[1−6] However, the particular mode of pattern formation that results from the oscillatory instability with finite wavelength (wave instability) has received relatively little attention.

Recently we have developed a simple reaction−diffusion model that contains a relatively large domain of the wave instability:

$$\frac{\partial x}{\partial t} = m\left(-xy^2 + z^2 - \frac{ax}{g+x}\right) + d_x\frac{\partial^2 x}{\partial r^2}$$

$$\frac{\partial y}{\partial t} = n(xy^2 - y + b) + d_y\frac{\partial^2 y}{\partial r^2} \qquad (1)$$

$$\frac{\partial z}{\partial t} = x - z + \frac{\partial^2 z}{\partial r^2}$$

The model can generate traveling and standing waves, asymmetric standing−traveling wave patterns, and target patterns.[7] It has also been shown that the wave instability can generate modulated traveling waves in unbounded systems.[8] Weakly modulated standing waves have been found in a model of CO oxidation on Pt in the vicinity of the codimension-two Hopf bifurcation.[9]

Here we present a study of pattern formation in model (1) with zero flux boundary conditions when the length of the system (L) is small, up to $1.5\lambda_c$, where λ_c is the characteristic wavelength of the wave instability. We show that in this case self-modulated standing waves appear.

Methods of Simulation

Simulations of the one-dimensional reaction−diffusion system are performed using a finite-difference approximation to eq 1. The corresponding system of ordinary differential equations is solved with the LSODE subroutine,[10] using numerical estimates of the Jacobian matrix. The error tolerances are 1×10^{-8} relative and 1×10^{-12} absolute. We use 256 grid points in all simulations, and the system length varies from 0.9 to 4.6. In most of our simulations we employ as initial conditions the homogeneous steady state, locally perturbed by increasing the value of y by 0.2 at the point on the wall and by 0.1 at the adjacent point. Zero flux boundary conditions are used in all simulations.

We employ a fast Fourier transform (FFT) program[11] to obtain two-dimensional Fourier spectra of the spatiotemporal patterns. This program requires the number of sampled points to be a power of 2, and we choose it equal to 256 for each dimension. We set the time step of sampling equal to 0.1 time units for all patterns analyzed.

To obtain Fourier spectra with the explicit fundamental wavenumber component in the cases of the half-wavelength patterns, we applied the FFT to one-wavelength patterns constructed by appending a duplicate of the original half-wavelength patterns, given by $x(L+r,t) = x(L-r,t)$, where r is in the interval $(0,L)$ and L is the original system length. This approach exploits the mirror symmetry resulting from the zero flux boundary conditions.

Results

Parametric Diagram of the System. Here we set $d_x = d_y = 0$, which gives the largest domain of the wave instability. We keep constant the following parameters: $g = 1 \times 10^{-4}$, $a = 0.9$, $b = 0.2$, $n = 15.5$, and vary the length of the system L and the parameter m. The value $m_c \approx 28.569\,15$ corresponds to the wave bifurcation and $m_h \approx 26.797\,67$ to the spatially independent Hopf bifurcation.[7] We refer to $\epsilon = (m_c - m)/m_c$ as the overcriticality.

Figure 1 shows a structure diagram in the ϵ,L-plane. At very small lengths ($L < 1.1$) the only stable modes are the spatially uniform steady or spatially uniform bulk oscillations, depending on ϵ. Standing waves (SW) occupy the largest part of the diagram. $SW_{0.5}$ stands for half-wavelength SW, SW_1 is one-wavelength SW, and $SW_{1.5}$ is three-halves-wavelength SW.

We have found two domains of modulated standing waves (MSW). One domain (MSW_1) separates the $SW_{0.5}$ and SW_1 domains; another domain (MSW_2) is situated inside the region of standing−traveling waves (STW). The latter are described in detail in our previous paper.[7]

Simple and Modulated Standing Waves. Figure 2 shows r,t-plots of the stable patterns at several lengths L in the range from 1.6 to 2.4, and $m = 20$ ($\epsilon \approx 0.3$). $SW_{0.5}$ is stable at $L = 1.6$ (Figure 2a). When the system length increases, the simple

[⊗] Abstract published in *Advance ACS Abstracts,* March 15, 1996.

0022-3654/96/20100-6604$12.00/0

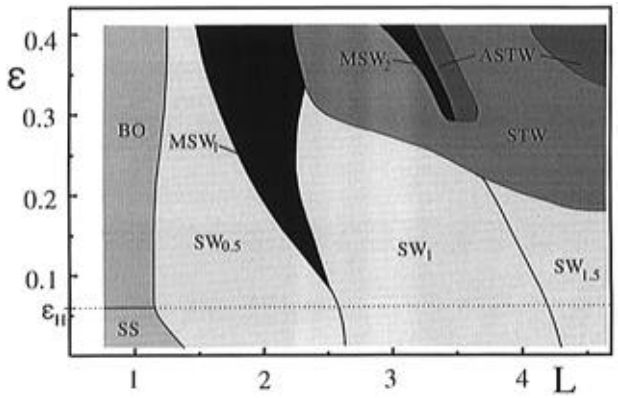

Figure 1. Structure diagram in the ϵ,L-plane. ϵ is overcriticality; L is the system length. SS designates the spatially uniform steady state; BO, spatially uniform bulk oscillations; SW_i, standing waves, index i indicates number of wavelengths; MSW_j, modulated standing waves; STW, standing−traveling waves; ASTW, aperiodic patterns of STW; ϵ_H corresponds to the space independent Hopf bifurcation.

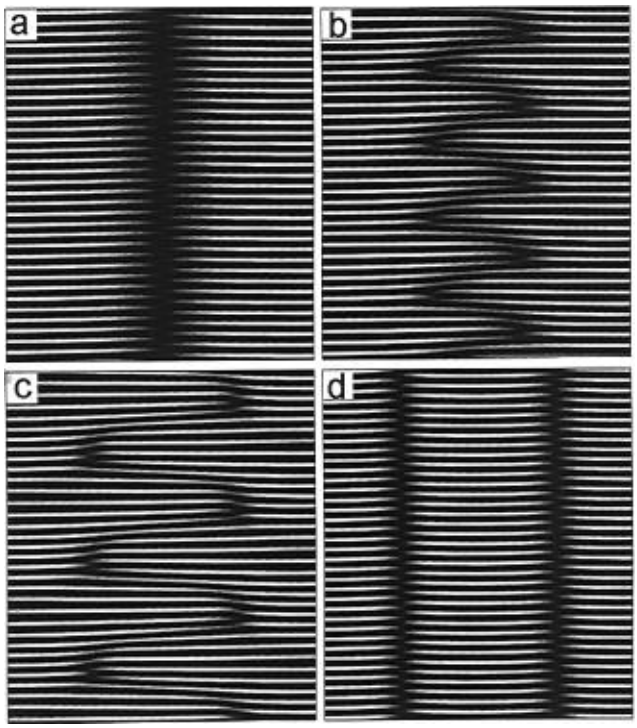

Figure 2. Simple and modulated standing waves: r,t-plots, $m = 20$ ($\epsilon \approx 0.3$), $L =$ (a) 1.6; (b) 1.8; (c) 2.2; (d) 2.4. The vertical axis is the time axis with initiation at the top; each frame corresponds to 25 time units. Values of x are quantified with 256 gray levels; white levels correspond to the maximum value of x; and black to the minimum value.

standing wave ($SW_{0.5}$) becomes unstable and the stationary node in the middle of the system disappears. Short-lived nodes emerge instead and alternate between the left and the right side of the system and at equal distance from the system center (Figure 2b; $L = 1.8$). This phenomenon heralds the emergence of modulated standing waves (MSW_1). As the system length increases, the distance between the alternating nodes also increases (Figure 2c; $L = 2.2$) and approaches the half-wavelength ($\lambda/2$). Stable SW_1 emerges with further increases of the system length (Figure 2d; $L = 2.4$).

As L is increased, the positions of the alternating MSW nodes undergo a continuous transition between the positions of the stationary nodes of $SW_{0.5}$ and SW_1, while the distance between the alternating nodes increases from 0 to $\lambda/2$. Overlays of 80 consecutive profiles (Figure 3) show the alternating nodes and

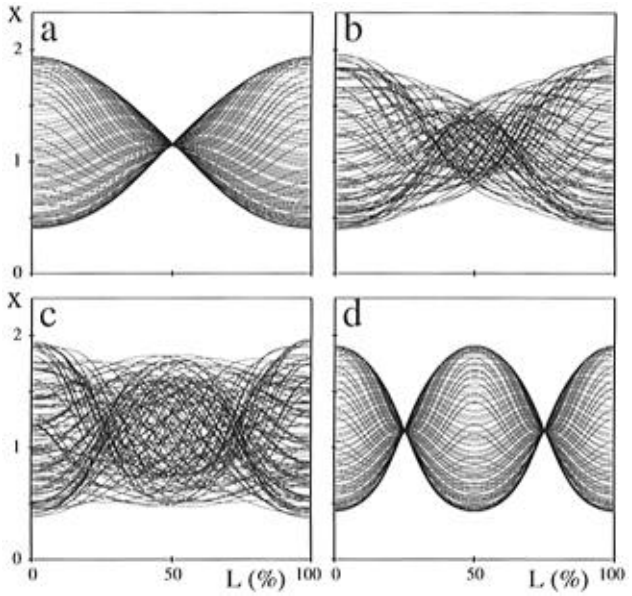

Figure 3. Simple and modulated standing waves corresponding to the patterns in Figure 2. Overlays of 80 consecutive profiles with step $\delta t = 0.05$.

demonstrate that the envelopes preserve the even parity of the envelopes of the simple SW.

To analyze the spatiotemporal patterns and evaluate intrinsic frequencies and characteristic wavenumbers, we employ two-dimensional Fourier transforms. Figure 4 shows the central regions of the two-dimensional Fourier spectra, which contain the major components of the patterns shown in Figures 2 and 3. The three-dimensional plots show the absolute values of the amplitudes and reveal both the major and minor components of the spectra. The two-dimensional plots display the positions of the major components in the plane of the space ($k/2\pi$) and time (f) frequencies. The spectra in Figure 4 are symmetric, and we need only consider the components with $k \geq 0$, since each component with a positive wavenumber has its counterpart with the corresponding negative wavenumber.

The spectra of $SW_{0.5}$ and SW_1 are simpler than those of MSW_1. Figure 4a shows the spectrum of $SW_{0.5}$ for $L = 1.6$, with the largest peak at frequency $f_1 = 1.289$ and wavenumber $k_1 = (2\pi)0.3125$, corresponding to wavelength $\lambda_1 = 2L$. The spectrum also contains second harmonics ($2k_1$, $2f_1$) of the right-bound and left-bound traveling waves and zero mode component (0, $2f_1$). Other large amplitude peaks are located at ($2k_1$, 0) and ($3k_1$, f_1). The spectrum of SW_1 ($L = 2.4$; Figure 4d) has its principal peak at $k_1 = (2\pi)0.4167$, $f_1 = 1.406$, and contains the same major components as $SW_{0.5}$: (k_1, f_1), ($2k_1$, $2f_1$), (0, $2f_1$), ($2k_1$, 0), and ($3k_1$, f_1); the last component is not shown in Figure 4d.

The spectra of the modulated SW are more complex than those of the simple SW. The spectrum of MSW_1 ($L = 1.8$; Figure 4b) contains a principal peak with wavenumber $k_1 = (2\pi)0.2778$, which corresponds to wavelength $\lambda_1 = 2L$, and intrinsic frequency of oscillations $f_1 = 1.289$, which is the same as for $SW_{0.5}$ ($L = 1.6$). There are also major components ($2k_1$, $2f_1$), (0, $2f_1$), and ($3k_1$, f_1) which are present in the spectra of the simple SW, and additionally a peak at (k_1, $2f_1$).

New components, characteristic of the spectra of MSW, are those associated with the self-modulation: (0, f_1-f_m) and ($2k_1$, f_1+f_m), where the frequency $f_m = 0.196$ is equal to the inverse period of appearance of the alternating nodes (see Figure 2b).

As the distance between alternating nodes of MSW_1 increases with the increasing system length, the amplitudes of the peaks

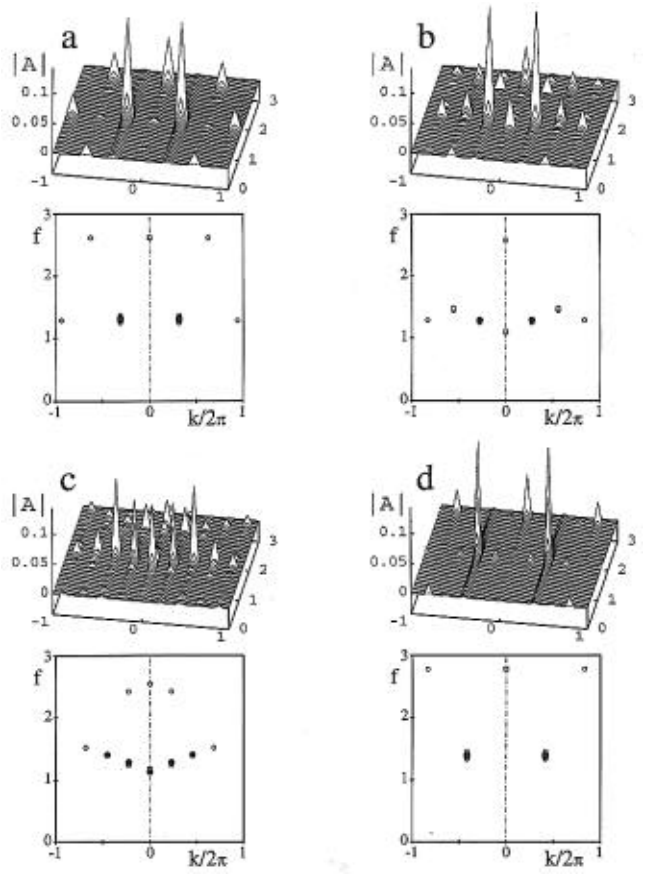

Figure 4. Two-dimensional Fourier spectra of the simple and modulated standing waves corresponding to the patterns in Figure 2. Top parts show the absolute values of the amplitude $|A|$; the bottom parts display the major components in the k,f-plane. Symbols indicate the amplitude of major components: (○) $0.03 \le |A| < 0.05$, (□) $0.05 \le |A| < 0.1$, (●) $0.1 \le |A|$.

at $(0, f_1-f_m)$ and $(2k_1, f_1+f_m)$ also increase. For $L = 2.2$ (Figure 4c), the spectrum has peaks corresponding to $k_1 = (2\pi)0.2273$, $f_1 = 1.289$, and $f_m = 0.137$. In this case, the amplitudes of the components $(0, f_1-f_m)$ and $(2k_1, f_1+f_m)$ are larger than that of the peak at (k_1, f_1). The spectrum also shows that the component $(3k_1, f_1+2f_m)$ replaces the component $(3k_1, f_1)$ that is present in the spectra of simple SW.

Besides the stable MSW, we have found long lasting transient MSW in the region near the boundary between the $SW_{0.5}$ and SW_1 domains below the MSW_1 domain and also near the boundary between the SW_1 and $SW_{1.5}$ domains. Fourier spectra of the transient MSW contain the same major components as the spectra of the stable MSW.

Modulated Standing Waves within the Domain of the Standing−Traveling Waves. There is another region of MSW in the $\epsilon-L$ diagram (Figure 1) that we designate as MSW_2. The region of MSW_2 is embedded in a domain of standing−traveling waves (STW) together with an adjacent region of aperiodic STW (ASTW).[7] Figure 5 illustrates the transition from STW ($m = 20$; $L = 3.3$), to MSW_2 ($L = 3.4$), and then to ASTW ($L = 3.6$). The STW (Figures 5a−c) is rather close to $SW_{1.5}$ with a slight prevalence of the left-bound traveling component wave, which is possible to see by comparison of Figure 5c to Figure 4d. The envelope of the STW constructed from overlays of 40 consecutive profiles shows two minima at fixed positions and three maxima, one close to the middle and two at the boundaries (Figure 5b). The Fourier spectrum of MSW_2 (Figure 5f) retains the core of the symmetric spectrum of MSW_1 (Figure 4b,c), with major peaks located at $(0, f_1-f_m)$, $(\pm k_1, f_1)$, and $(\pm 2k_1, f_1+f_m)$, where $k_1 = 0.2942$, $f_1 = 1.328$, and $f_m = 0.137$. The overlays of 80 consecutive profiles demonstrate the even parity of the envelope of MSW_2.

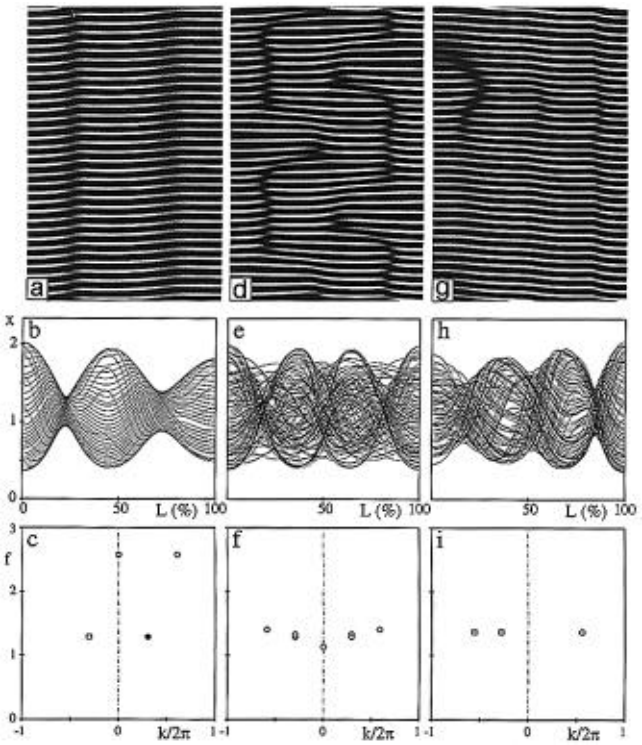

Figure 5. Space−time (r,t) plots of a standing−traveling wave (STW), a modulated standing wave (MSW_2), and an aperiodic STW shown together with overlays of consecutive profiles and Fourier spectra. The r,t-plots correspond to 25 time units; the time axis is vertical with initiation at the top. The overlays contain 40 (b) and 80 (e, h) consecutive profiles with step 0.08. The Fourier spectra (c, f, i) display the major components with absolute values of the amplitude $|A|$: (○) $0.03 \le |A| < 0.05$, (□) $0.05 \le |A| < 0.1$, (●) $0.1 \le |A|$. $m = 20$, L = (a, b, c) 3.3; (d, e, f) 3.4; (g, h, i) 3.6.

The characteristic feature of the ASTW is the appearance of the second space subharmonics $(k_1/2, f_1)$ of the more powerful right-bound traveling component wave (Figure 5i). The envelope of the ASTW differs from that of the periodic STW. The sharp fixed locations of minima and maxima on the envelope in the case of STW become less pronounced in the case of ASTW.

Discussion

The core of the Fourier spectra of modulated standing waves MSW_1 and MSW_2 consists of five components: $(0, f_1-f_m)$, $(\pm k_1, f_1)$, and $(\pm 2k_1, f_1+f_m)$. Symmetry considerations permit us to restrict our analysis to the three components with wavenumbers 0, k_1, and $2k_1$. To elucidate the role of these three components, we truncate the spectrum of the pattern shown in Figure 2c, removing smaller amplitude components step by step. After each step, the truncated spectrum is converted to the corresponding time−space pattern via the inverse Fourier transform. Figure 6 shows several results of the procedure. Elimination of all components with amplitudes less than 0.002 in absolute value results in a pattern (Figure 6a) that is nearly indistinguishable from the original one (Figure 4c). Figure 6b shows the components used for reconstruction of the pattern by the inverse Fourier transform. Elimination of all components with amplitudes less than 0.01 leads to the appearance of minor artifacts (Figure 6c,d). With the spectrum consisting only of the five (three with $k \ge 0$) major components (Figure 6f), the artifacts become more pronounced (Figure 6e); nevertheless, the basic

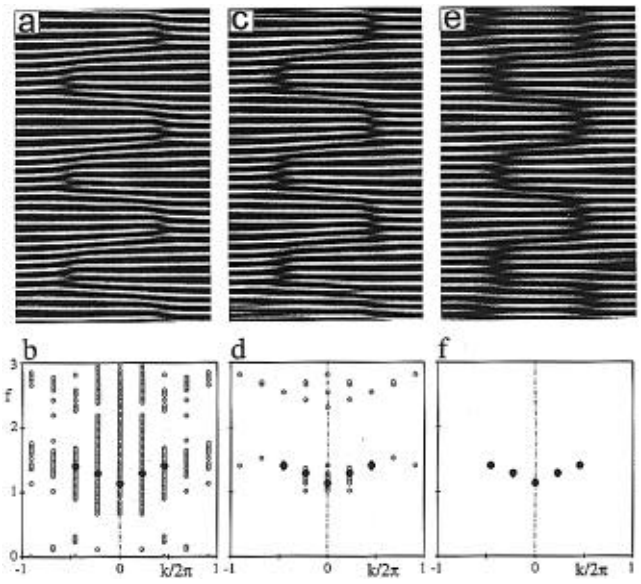

Figure 6. Space−time plots of reconstructed modulated standing wave (MSW_1) and corresponding components used in the inverse Fourier transform, $m = 20$, $L = 2.2$. The time axis in the r,t-plot is the vertical axis with initiation at the top and represents 25 time units. The components used in the inverse transform have $|A|$ larger than (a, b) 0.002, (c, d) 0.01, (e, f) 0.05. The spectra (b, d, f) indicate all components used to reconstruct the pattern. Absolute values of the amplitudes are characterized by symbols: (○) $|A| < 0.1$, (●) $0.1 \leq |A|$.

pattern of alternating modes remains qualitatively the same. Fourier spectra of modulated convection waves in a rotating Couette system display similar properties.[12]

The reduction of the spectrum to three components makes it possible to compare it with the spectrum of a conventional modulated traveling wave. The latter consists of a central carrier mode and two sidebands. The difference between the frequency of a side mode and that of the central one is equal to the frequency of modulation. In nondispersive media that permit transmission of acoustic or radio signals without distortion, the speeds of all modes are equal. That is, all wavenumbers are proportional to the corresponding frequencies. The core of our modulated waves also consists of three components, with the principal mode (k_1, f_1) playing the role of the carrier wave, and two side modes: (0, f_1-f_m) and ($2k_1$, f_1+f_m). The frequency relations of the side modes to the central one are the same as in a conventional modulated wave. However, the relations of the wavenumbers are completely different. Because the modes must match the system length, the wavenumbers can differ only by nk_1, where n is a whole number. As a result, in our case, the left-side mode is a zero mode, and the right-side one has a wavelength which is half that of the central mode and equal to the system length.

Our simulations show that patterns rather close to those of MSW_1 can be obtained using only two modes: the basic one (k_1, f_1) and the side mode ($2k_1$, f_1+f_m).

Standing waves have been observed in experiments on catalytic heterogeneous reactions with global coupling.[13,14] Modulated standing waves were found in models of catalytic reaction−diffusion systems with global coupling[9,15,16] and in the Ginzburg−Landau equations.[17,18]

The modulated standing waves shown in Figure 2b,c qualitatively resemble some of the spatiotemporal patterns found by Middya et al.[15,16] (Figure 14 in ref 15 and Figure 12 in ref 16). The differences between the patterns probably arise from the details of the models employed. Middya et al.[15,16] used reaction−diffusion models with local kinetics of the generalized Van der Pol type and global coupling. In our model the core oscillator is of the Brusselator type, and rapid diffusion is responsible for the long-range spatial coupling.

Acknowledgment. We gratefully acknowledge the support of the National Science Foundation Chemistry Division and the W. M. Keck Foundation.

References and Notes

(1) Nicolis, G.; Prigogine, I. *Self-Organization in Nonequilibrium Systems*; Wiley: New York, 1977.

(2) Haken, H. *Synergetics*; Springer: Berlin, 1978.

(3) Kuramoto, Y. *Chemical Oscillations, Turbulence and Waves*; Springer: Berlin, 1984.

(4) Ross, J.; Müller, S. C.; Vidal, C. *Science* **1988**, *240*, 460.

(5) *Waves and Patterns in Chemical and Biological Media*; Swinney, H. L., Krinsky, V. I. Eds.; *Physica D* **1991**, *49* (1 & 2).

(6) *Chemical Waves and Patterns*; Kapral, R., Showalter, K. Eds.; Kluwer: Dordrecht, 1995.

(7) Zhabotinsky, A. M.; Dolnik, M.; Epstein, I. R. *J. Chem. Phys.* **1995**, *103*, 10306.

(8) Malomed, B. A. *Z. Phys. B* **1984**, *55*, 241.

(9) Levine, H.; Zhou, X. *Phys. Rev. E* **1993**, *48*, 50.

(10) Hindmarsh, A. C. In *Scientific Computing*; Stepleman, R. S., et al., Eds.; North-Holland: Amsterdam, 1983; p 55.

(11) Press, W. H.; Flannery, B. P.; Teukolsky, S. A.; Vetterling, W. T. *Numerical Recipes*; Cambridge University Press: Cambridge, 1986.

(12) Takeda, I.; Fisher, W. E.; Sakabara, J. *Science* **1994**, *263*, 502.

(13) Cordonier, G. A.; Schuth, F.; Schmidt, L. D. *J. Chem. Phys.* **1989**, *91*, 5374.

(14) Jakubith, S.; Rotermund, H. H.; Engel, W.; von Oertzen, A.; Ertl, G. *Phys. Rev. Lett.* **1990**, *65*, 3013.

(15) Middya, U.; Graham, M. D.; Luss, D.; Sheintuch, M. *J. Chem. Phys.* **1993**, *98*, 2823.

(16) Middya, U.; Luss, D.; Sheintuch, M. *J. Chem. Phys.* **1994**, *101*, 4688.

(17) Cross, M. C. *Phys. Rev. A* **1988**, *38*, 3593.

(18) Mertens, F.; Imbihl, R.; Mikhailov, A. *J. Chem. Phys.* **1994**, *101*, 9903.

JP9532982